# The structure and metal binding properties of *Chlamydia trachomatis* YtgA

Zhenyao Luo [1,2,3], Stephanie L. Neville [4,5], Rebecca Campbell [5], Jacqueline R. Morey [5], Shruti Menon [6], Mark Thomas [7], Bart A. Eijkelkamp [5], Miranda P. Ween [5], Wilhelmina M. Huston [7], Bostjan Kobe [1,2,3*], Christopher A. McDevitt [4,5*]

1. School of Chemistry and Molecular Biosciences, University of Queensland, Brisbane, Queensland, Australia.
2. Australian Infectious Diseases Research Centre, University of Queensland, Brisbane, Queensland, Australia.
3. Institute for Molecular Bioscience, University of Queensland, Brisbane, Queensland, Australia.
4. Department of Microbiology and Immunology, The Peter Doherty Institute for Infection and Immunity, University of Melbourne, Melbourne, Victoria, Australia
5. School of Biological Sciences, University of Adelaide, Adelaide, South Australia, Australia.
6. School of Biomedical Sciences, Queensland University of Technology, 2 George St, Brisbane, QLD 4001 (formally at)
7. School of Life Sciences, University of Technology Sydney, 15 Broadway, Ultimo, NSW, Australia

*Address correspondence to Christopher A. McDevitt, Department of Microbiology and Immunology, The Peter Doherty Institute for Infection and Immunity, University of Melbourne, Melbourne, Victoria, 3000, Australia. Phone: 61-3-8344-7200. E-mail: christopher.mcdevitt@unimelb.edu.au; and Bostjan Kobe, School of Chemistry and Molecular Biosciences, University of Queensland, Brisbane, Queensland, Australia. Phone: 61-7-3365-2132. E-mail: b.kobe@uq.edu.au

26

27 Running Head: Structure and metal-binding properties of YtgA

**ABSTRACT**

The obligate intracellular pathogen *Chlamydia (C.) trachomatis* is a globally significant cause of sexually transmitted bacterial infections and the leading etiological agent of preventable blindness. The first-row transition metal iron (Fe) plays critical roles in chlamydial cell biology and acquisition of this nutrient is essential for the survival and virulence of the pathogen. Nevertheless, how *C. trachomatis* acquires Fe from host cells is not well understood, as it lacks genes encoding known siderophore biosynthetic pathways, receptors for host Fe-storage proteins, and the Fe acquisition machinery common to many bacteria. Recent studies have suggested that *C. trachomatis* directly acquires host Fe via the ATP-binding cassette permease YtgABCD. Here, we characterised YtgA, the periplasmic solute binding protein component of the transport pathway, that has been implicated in scavenging Fe(III) ions. The structure of Fe(III)-bound YtgA was determined at 2.0 Å resolution with the bound ion coordinated via a novel geometry (N3O2). This unusual coordination suggested a highly plastic metal-binding site in YtgA capable of interacting with other cations. Biochemical analyses showed that the metal-binding site of YtgA was not restricted to interaction with only Fe(III) ions, but could bind all transition metal ions examined. However, only Mn(II), Fe(II) and Ni(II) ions bound reversibly to YtgA, with Fe being the most abundant cellular transition metal in *C. trachomatis*. Collectively, these findings show that YtgA is the metal-recruiting component of the YtgABCD permease and is most likely involved in acquisition of Fe(II) and Mn(II) from host cells.

**KEYWORDS**

YtgA; solute-binding protein; *Chlamydia trachomatis;* iron acquisition; ABC transporter

## INTRODUCTION

Iron (Fe) is an essential micro-nutrient for nearly all forms of life (1-3). In prokaryotes, Fe is frequently employed as a cofactor in redox-dependent processes or in central biochemical pathways, including aerobic respiration, DNA repair, and cellular metabolism (4-6). *Chlamydia* (*C.*) *trachomatis* is the causative agent of the most prevalent bacterial sexually transmitted infection worldwide and the leading cause of preventable blindness (7, 8). It is estimated that more than 100 million new chlamydial infection cases are diagnosed annually worldwide (9). As an obligate intracellular pathogen, this Gram-negative bacterium invades and grows within eukaryotic cells, and scavenges nutrients from the intracellular environment of the host cells (10, 11). Analysis of the *C. trachomatis* genome reveals that despite its small genome of ~1 megabase pairs, *C. trachomatis* possesses the genes that encode a complete aerobic respiratory chain that includes sodium-motive NADH-quinone oxidoreductase, succinate dehydrogenase, and the cytochrome bd complex (12), all of which are Fe-containing proteins. This implies that Fe is required for chlamydial cellular metabolism. Additionally, functional studies have provided evidence for an Fe requirement in host cell interaction. Starvation of Fe forces *C. trachomatis* to enter a metabolically active, yet non-infectious reticulate body form (13), with reversion to the infectious form upon relief of Fe-restrictive conditions (14). Collectively, these data indicate that Fe acquisition is essential for *C. trachomatis* survival and pathogenicity.

In biological systems, Fe commonly exists in two oxidative states: ferrous [Fe(II)] or ferric [Fe(III)]. Prokaryotic acquisition of Fe is predominantly facilitated by siderophores and their receptors that capture and internalise Fe(III) from the extracellular environment (15) and/or surface receptors that capture Fe-containing proteins/molecules from the host, such as transferrin, lactoferrin, and haem (16). Some bacteria are also capable of directly acquiring Fe in the ferrous form through transporters such as FeoABC from *Escherichia coli* K12 (17), and

YfeABC from *Yersinia pestis* (18). Genome sequencing has revealed that *C. trachomatis* does not encode protein homologs of known siderophore biosynthetic pathways or surface receptor proteins involved in scavenging host-iron storage proteins/haem, which are common components of Fe acquisition systems in other bacteria. To date, the only putative Fe acquisition system identified in *C. trachomatis* is YtgABCD, which is comprised of YtgA, a periplasmic solute-binding protein (SBP), and YtgBCD, a cytoplasmic membrane localised ATP-binding cassette (ABC) transporter. Sequence analyses of YtgA indicate that it shares homology with the ABC transporter SBPs involved in the recruitment of metal ions (cluster A-I) and metal chelates (cluster A-II). Prior studies of YtgA have proposed that the protein is specific for Fe(III) (19). However, the amino acid composition of the presumptive metal-binding site and the associated bioinorganic chemistry strongly suggest that YtgA may have the capacity to interact with other first row transition metal ions such as Mn(II), but this has remained poorly defined.

In this work, we combined X-ray crystallography with differential scanning fluorimetry and metal-binding assays to elucidate the structural and metal-binding properties of *C. trachomatis* serovar D/UW-3/Cx YtgA. We report the first high resolution structure of the protein, determined to 2.0 Å resolution in the Fe(III)-bound state. Although YtgA shares a common fold with other members of the cluster A-I subgroup of SBPs, we show that the protein has a highly plastic metal-binding site capable of offering a range of coordination geometries. Analyses of the metal-binding properties of the YtgA revealed that it was highly permissive for interaction with a broad range of transition metal ions including Mn(II), Fe(II), Co(II), Ni(II), and Zn(II). Nevertheless, functional specificity in the YtgABCD permease most likely arises from only a subset of these metal ions [Fe(II), Mn(II) and Ni(II)] being readily released from YtgA once bound.

## RESULTS

### YtgA belongs to a subgroup of SBPs with broad ligand specificity

Comparative sequence analysis of *C. trachomatis* YtgA with 31 functionally characterized cluster A-I and A-II SBPs revealed that the protein clustered with a subgroup of cluster A-I SBPs that have broad ligand specificity [i.e. interaction with Mn(II), Fe(II) and/or Zn(II)] (**Fig. 1a**). This subgroup shares sequence identities of ≥ 20% over the core protein fold (over > 200 amino acids) and is distinct from the Fe-recruiting cluster A-II SBPs, which bind metal-chelates, and the closely related Zn(II)-specific cluster A-I SBPs. Notably, Zn(II)-specific SBPs frequently possess an acidic amino acid enriched region that is absent from YtgA (**Fig. 1b**) (20, 21). YtgA orthologs from other chlamydial species, namely *C. muridarum*, *C. suis*, *C. psittaci*, and *C. pneumoniae*, share sequence identities ranging from 57% to 85% (over > 300 amino acids). Notably, the metal-binding site residues in YtgA orthologs are strictly conserved (**Fig. 2**). Taken together, these data suggest that YtgA directly interacts with the ionic form of metals and may not be restricted to binding only Fe(III) ions as previously reported (19).

### YtgA interacts with a broad range of divalent transition metal ions

To investigate the metal binding properties of *C. trachomatis* YtgA, we expressed a recombinant C-terminal dodecahistidine-tagged variant without the putative Sec-type signal peptide (residues 34-326) (22). Recombinant YtgA was purified by immobilized metal affinity chromatography, the affinity tag removed, and the protein further purified by size exclusion chromatography (SEC) (**Fig. 3a**). SEC showed that recombinant YtgA was isolated as a single monodisperse species with a relative molecular mass of 36.2 kDa (based on molecular mass standards), which matched closely with the predicted molecular mass (36.1 kDa) of recombinant, tag-cleaved monomeric YtgA (**Fig. 3b**). Endogenous metals, which may have co-purified, were removed by denaturation at pH 4.0 in the presence of 20 mM

127 ethylenediaminetetraacetic acid (EDTA) prior to refolding by dialysis in 20 mM Tris-HCl, pH
128 7.2, 200 mM NaCl. Inductively coupled plasma-mass spectrometry (ICP-MS) analysis of
129 refolded, tag-cleaved YtgA found that it was metal-free, containing less than 0.01 mol of metal
130 ions per mol of protein.

131 The interaction of recombinant YtgA with metal ions was first assessed by differential
132 scanning fluorimetry (DSF) using the environmentally sensitive probe SYPRO Orange (23).
133 DSF was performed with a range of physiologically relevant metal ions [Mg(II), Ca(II), Mn(II),
134 Fe(II), Fe(III), Co(II), Ni(II), Cu(II) and Zn(II)] to ascertain which metals interacted with the
135 protein. We also examined interaction with Cd(II), as this metal has been shown to bind to a
136 related cluster A-I SBP (23). DSF analyses revealed that metal-free YtgA had a $T_m$ of 50.5 ±
137 0.9 °C (**Table 1, Fig. 4**). Treatment with a 10-fold molar excess of Mg(II), Ca(II) or Fe(III) did
138 not significantly alter the $T_m$ of the protein (**Table 1, Fig. 4**; $\Delta T_m$ ± S.D. ≤ 2 °C; $P > 0.05$).
139 Modest, but significant shifts in the $T_m$ of YtgA were observed with Mn(II), Fe(II) and Ni(II)
140 ($P < 0.001$), while larger shifts (>10 °C) were observed for Co(II), Zn(II) and Cd(II) ions ($P <$
141 0.001). Although interaction of Cu(II) with YtgA was tested, addition of Cu(II) resulted in
142 precipitation of YtgA upon supplementation, thus data could not be collected. These data show
143 that YtgA is capable of interacting with a broad range of metal ions similar to other members
144 of the Mn/Zn/Fe clade of cluster A-I SBPs. However, these findings also contrast starkly with
145 those reported by Miller and co-workers, who concluded that YtgA was a specific Fe(III)-
146 binding SBP (19). We speculate that the interaction with Fe(III) with YtgA in that study may
147 be attributable to the higher ratio of metal to protein used. Consequently, we further analysed
148 YtgA and observed a modest positive shift in the protein $T_m$ (+6.3 °C) at higher Fe(III)-protein
149 ratios (≥ 100-fold molar excess, **Fig. 4h**). This data shows that Fe(III) can bind to YtgA,
150 although it may have a poor on-rate.
151

YtgA and Fe(II)

To complement the DSF analyses, we directly probed the metal-binding properties of YtgA by ICP-MS. Here, *in vitro* metal-binding assays were conducted using metal-free YtgA and a 10-fold molar excess of the transition metal ions Mn(II), Fe(II), Fe(III), Co(II), Ni(II), Zn(II) and Cd(II). ICP-MS analyses revealed that YtgA bound all metal ions with stoichiometries of ~1 mol metal ion per mol of protein (**Fig. 5**). Thus, our data show that the metal-binding site of YtgA is capable of binding one metal ion per protein molecule and is not restricted to interaction with only Fe(III) ions. We then assessed the stability of the YtgA-metal complexes by treatment with a 100-fold molar excess of the strong chelating agent EDTA, which has affinities for transition metal ions in the range of ~$10^{-13}$ to $10^{-25}$ M (24). The affinities of cluster A-I SBPs for metal ions are several orders of magnitude less and are typically in the range of ~$10^{-7}$ to $10^{-9}$ M (20, 25). Here, we observed that the metal ions Mn(II), Fe(II) and Ni(II) were efficaciously removed by EDTA (**Fig. 5**). This result contrasts starkly with Fe(III), Co(II), Zn(II) and Cd(II), which formed YtgA-metal complexes with that were essentially irreversible (extraction ≤ 15%) (**Fig. 5**). These ions were only extracted from YtgA by unfolding the protein in the presence of EDTA. It is a physiological requirement for transport that the bound metal ion can be readily released from the SBP to the transporter. Taken together, our data suggest that Mn(II), Fe(II) and Ni(II) are potential physiological ligands of YtgA. By contrast, although Fe(III), Co(II) and Zn(II) can bind to YtgA, the stabilities of the resultant protein-metal complexes are unlikely to permit release of the ions to the YtgBCD transporter for cytoplasmic import.

To better understand the physiological context of YtgA and metal transport we performed whole cell ICP-MS on *C. trachomatis* infectious elementary bodies (EB). This revealed that Fe was the most abundant transition metal ion (**Fig. 6**) with the other metals having lower abundance, which can be summarised as: Fe > Zn > Cu > Mn > Ni. Therefore,

177 the cellular analyses imply that YtgA most likely facilitates Fe(II) acquisition for *C.*
178 *trachomatis*.
179
180 **Structural analyses of YtgA**
181 To further our understanding of *C. trachomatis* YtgA, a high-resolution structure of the protein
182 was determined by X-ray crystallography. Although crystallization of the protein with Fe(II),
183 the presumptive physiological ligand, was attempted, oxidation to Fe(III) occurred during the
184 crystallization process, based on the observed solution colour. The YtgA crystal diffracted to
185 2.0 Å resolution. One molecule of YtgA was present in each asymmetrical unit. Residues 34-
186 39 and 285-286 were not modelled in the refined structure due to a lack of electron density in
187 the corresponding regions. Crystallographic refinement statistics are summarized in **Table 2**.
188 YtgA comprises two globular domains, denoted as N- and C-terminal domains, and a
189 domain-linking helix (α6) that spans the entire molecule (**Fig. 7a, b**). Similar to other cluster
190 A-I SBPs, the inter-domain helix would most likely preclude large conformational motion of
191 either domain, as reported for *S. pneumoniae* PsaA (26) and *Yersinia pestis* YfeA (27). This is
192 in stark contrast to the shorter, flexible inter-domain linkages present in non-metal binding
193 SBPs, such as the amino acid-binding SBP LivJ (28, 29), that permit larger movement (up to
194 60°) of the two domains. In YtgA, the N- and C-terminal domains both comprise five α-helices
195 (N-terminal: α1, 2, 3, 4 and 5; C-terminal: α7, 8, 9, 10 and 11) that each flank a four-stranded
196 β-sheet (N-terminal: β1, 2, 3, and 4; C-terminal: β5, 6, 7 and 8) at the centre (**Fig. 7a, b**). The
197 metal-binding site resides at the interface between the two domains and is located
198 approximately 10 Å beneath the molecular surface of the protein. One Fe(III) ion, with full
199 occupancy, is present at the metal-binding site of the protein, with the two globular domains
200 closed over this region. In related cluster A-I SBPs, such as *Streptococcus pneumoniae* PsaA,
201 this conformation represents the closed, ligand-bound form of the protein and is distinct from

the open, metal-free state (30). In YtgA, the loop connecting α9 and β6 on the surface of the C-terminal domain dwells directly above the bound Fe(III) ion. Together, these features bury the metal ion and the binding-site, shielding them from the bulk solvent in the closed, metal-bound state (**Fig. 7c**). In the binding site, the bound Fe(III) ion forms coordination interactions with the Nε2 atoms from His75, His141 and His207, and the Oδ1 and Oδ2 atoms from Asp299, with the coordination bond lengths of 2.04, 2.14, 2.21, 2.01, and 2.38 Å, respectively, thus giving a distorted N3O2 trigonal bipyramidal coordination geometry to the bound metal ion (**Fig. 7d**).

Overall, YtgA possesses a structural fold highly conserved among cluster A-I SBPs**,** including *Treponema pallidum* Zn(II)-binding SBP TroA (31) (**PDB: 1TOA**), *Streptococcus pyogenes* Fe(II/III) SBP MtsA (32) (**PDB: 3HH8**), *Yersinia pestis* Fe/Mn(II) SBP YfeA (27) (**PDB: 5UY4**), *Staphylococcus aureus* Mn(II)-binding SBP MntC (33) (**PDB: 4K3V**), *Staphylococcus pseudintermedius* Mn(II) SBP SitA (34) (**PDB: 4OXR**), and *S. pneumoniae* Mn(II)-binding SBP PsaA (35) (**PDB: 3ZTT**). Superimposing the crystal structures backbones revealed low rmsd values (< 1.1 Å) between YtgA and the other SBP structures (**Fig. 8a,b**, **Table 3**), despite the low level of overall sequence identity (< 26%) between them. Notably, three of the four metal-coordinating ligands in YtgA, namely, His75, His141 and Asp299, are strictly conserved through all cluster A-I SBPs compared in this study. Interestingly, the fourth metal-coordinating position in YtgA presents a histidine residue (His207), which resembles Zn(II)-specific SBPs, such as ZnuA and AdcAII, and TroA, which has been implicated as having a physiological role in Zn(II) acquisition (**Fig. 8c**). By contrast, structurally characterised SBPs that favour interaction with Fe, such as MtsA and YfeA (**Fig. 8d**), or Mn(II), such PsaA and MntC (**Fig. 8e**), present an acidic residue at this location. Another distinct structural feature of YtgA is that the protein possesses five helices in each of its globular domains, as opposed to the four -helices-per-domain arrangement observed in other

cluster A-I SBPs (**Fig. 8b**). The extra helices (α4 in the N-terminal domain and α8 in the C-terminal domain) are positioned on the same side of the molecule, relative to the domain-linking helix (**Fig. 8a, b**). Whether these extra structural elements play a role in cargo acquisition or recognition by YtgBCD permease, remains to be determined.

*S. pyogenes* MtsA and *Yersinia pestis* YfeA are among the cluster A-I SBPs that show binding preference for Fe(III) (27, 32). Comparing the metal-bound states of YtgA and MtsA shows that although a single Fe(III) ion is present in both structures and adopts a distorted trigonal bipyramidal coordination geometry, the coordinating ligands offered by the metal binding sites are distinctly different. In YtgA, the Fe(III) ion is coordinated by three N and two O atoms. By contrast, in MtsA, the bound Fe(III) ion is coordinated by two N and three O atoms. In YfeA, both the acidic residues in the metal-binding site contribute to bidentate coordination with Fe(III), resulting in a two-N, four-O (N2O4) trigonal prism geometry. Notably, the coordination environment present at the YtgA metal-binding site closely resembles that of the Zn(II)-binding SBPs and TroA (31, 36, 37). Although the coordination environment is similar, the acidic residue employs both oxygen atoms to bind Fe(III) in YtgA. This is in contrast to Zn(II)-specific SBPs, where only one oxygen atom from the carboxyl group on the acidic residue is involved in reversible Zn(II) ion coordination.

## DISCUSSION

Acquisition of Fe is essential for the survival and virulence of the obligate intracellular pathogen *C. trachomatis*. The scavenging of Fe and other crucial transition metal ions from the extra-cytoplasmic environment is most commonly facilitated in prokaryotes by cluster A-I SBPs. Iron uptake by *C. trachomatis* is associated with the YtgABCD permease, which has been shown to be regulated by Fe via the DtxR family regulator YtgR (38). Import of Fe was inferred to be facilitated by YtgA due to its previously reported interaction with Fe(III) (19). In this study, we have determined the first high-resolution structure of YtgA and, by combining *in vitro* metal binding and DSF assays, reveal that YtgA is a highly promiscuous SBP capable of interaction with a broad range of transition metal ions. These findings challenge earlier conclusions regarding the physiological ligand(s) of YtgA and the inferred specificity of the YtgABCD permease.

The selective import of metals ions by ABC permeases can be ascribed to the specificity of the cluster A-I SBP component. Specificity within these proteins arises from the coordinating environments offered by the metal-binding sites. First-row transition metals utilize their 3d-orbitals to form coordination bonds with ions that carry lone pair electrons, such as sulfur, oxygen, and nitrogen. The resultant complexes adopt specific spatial geometries due to the directionality of the metal ion 3d-orbitals. Analysis of the available Zn(II)-specific SBP crystal structures reveals that Zn(II) is most frequently associated with tetrahedral (4 ligands) complexes, owing to the small ionic radius of the ion. Further, as a soft Lewis acid, Zn(II) tends to interact with soft Lewis bases (39, 40), such as nitrogens in histidines. Mn(II) and Fe(II), which in contrast have larger ionic radii, can accommodate additional ligands with less repulsion energy penalty. Coordination numbers for these metal ions are frequently 5 and 6, with trigonal bipyramidal and octahedral geometries. Mn(II) and Fe(II) are hard Lewis acids that preferentially interact with hard Lewis bases (39, 40), such as the oxygen atoms from water

or carboxylate containing amino acids. The high resolution structure of YtgA shows that the metal-binding site is defined by three histidine residues (His75, His141, His207) and one aspartic acid residue (Asp299), resembling the binding sites frequently found in Zn(II)-specific SBPs such as *Salmonella* ZnuA (41). However, in YtgA, the conformation of Asp299 is not restricted as it is in other cluster A-I SBPs. Consequently, it allows one or both of the oxygen atoms in its carboxylate group to contribute to metal coordination. This arrangement would permit YtgA to provide tetrahedral (N3O1: 3 nitrogen atoms from His75, His141 and His207 and one oxygen atom from the monodentate interaction of Asp299), trigonal bipyramidal (N3O2: 3 nitrogen atoms from His75, His141, His207 and two oxygen atoms from the bidentate interaction of Asp299), or octahedral (N3O3: 3 nitrogen atoms from His75, His141, His207, two oxygen atoms from the bidentate interaction of Asp299 and one oxygen atom from a water molecule) metal ion coordination. The balance between the "hardness" and "softness" of the ligands can be fine-tuned by including or excluding extra coordinating oxygen atoms depending on the preference of the interacting metal ion. However, this flexible coordination geometry precludes the capacity for strict selection of only a single metal ion ligand.

The flexibility of YtgA Asp299 has similarity to Asp280 of *Streptococcus pneumoniae* PsaA (30). In PsaA, this equivalent carboxylate residue influences metal ion selection and reversibility of the metal-PsaA complex, resulting in impacts upon metal ion transport (23, 30, 35, 42). Consistent with these insights, YtgA was also shown to be highly promiscuous for interaction with a range of metal ions, despite their preference for distinct coordination geometries. Nevertheless, our analyses also revealed differences in the stabilities of the resultant YtgA-metal complexes. The metal ligands Co(II), Zn(II) and Cd(II) all form highly stable complexes with YtgA, as shown by the large $T_m$ shifts and inability of EDTA to extract the bound metal ion. Notably, we also observed that YtgA bound Fe(III) irreversibly, rendering Fe(III) an unlikely physiological ligand. This is consistent with the previous finding that YtgA

296 bound Fe(III) could not be replaced by $^{59}$Fe(III) (19). Interestingly, the metal ion did not
297 significantly shift the protein $T_m$ at similar concentrations to the other metal ligands. We
298 speculate that this may be due to a slow on rate; alternatively, it may reflect a solubility issue
299 associated with the $FeCl_3$ salt in the DSF assay. Irrespective of the precise technical basis for
300 this issue, our data indicate that YtgA stabilization with Fe(III), Co(II), Zn(II) and Cd(II) is
301 highly thermodynamically favourable.

302 Successful cellular import of transition metal ions is dependent not only on their
303 efficient binding by the SBP, but also subsequent release upon interaction with the ABC
304 transporter. Prior studies of related cluster A-I SBPs have shown that kinetically-trapped
305 protein-metal complexes are incapable of releasing the bound metal ions to the transporter (30,
306 35, 42). Therefore, we propose that Fe(III), Co(II), Zn(II) and Cd(II) are not transported ligands
307 of the YtgABCD permease. Further, these ions could potentially abrogate permease function
308 through the formation of irreversible metal-YtgA complexes. By contrast, Mn(II), Fe(II) and/or
309 Ni(II) are potential physiological ligands with Fe(II) the most likely ligand given the 19-fold
310 greater abundance of Fe(II) over Mn(II) in *C. trachomatis* cells. The cytosolic concentrations
311 of these metal ions within the eukaryotic host cell provide additional context for speculation
312 (43). In the cytosol, the labile pool of Fe(II) (0.1 -1 μM) and Mn(II) (1 μM (44)) is estimated
313 to be at least 4 orders of magnitude greater than Zn(II) (50 pM (45)), Co(II), Ni(II) and Cu(II)
314 ions. Although the relative abundance of metal ions within the membrane-bound compartment
315 occupied by *C. trachomatis* in the eukaryotic cell remains unknown, it likely reflects the
316 cytoplasmic abundance. Thus, we infer that the lower abundance of the labile forms of
317 competing metal ions would minimise their potential interactions with YtgA *in vivo*. The
318 balance of evidence indicates that YtgA is most likely involved in Fe(II) uptake, but we cannot
319 exclude the possibility that it also facilitates low-level Mn(II) uptake as well. Current literature
320 suggests that Chlamydiae may be able to acquire Fe(II) via the slow-recycling pathway of

endocytosed transferrin receptor (3, 46, 47). This system is assumed to rely on the reduction of transferrin-bound Fe(III) to Fe(II) via the host ferrireductase $STEAP_3$ (48) or possibly riboflavin (49), followed by endosome fusion with the chlamydial inclusion (46, 50, 51). Further, it has been suggested that the chlamydial inclusion may interact with both mitochondria and autophagosomes, to facilitate acquisition of essential nutrients (52, 53). Collectively, these mechanisms would allow *C. trachomatis* to scavenge Fe(II) from the host cytosol into the Chlamydiae inclusion environment, where it could be selectively transported by YtgABCD.

Given the high degree of sequence identities amongst YtgA orthologs, our observations suggest that chlamydial SBPs employ a common metal-binding mechanism. As Chlamydiae have a strict iron-dependency, the promiscuity of YtgA may arise from the composition of the metal-binding site and the associated bioinorganic limitations in achieving selectivity for Fe(II), thereby rendering it permissive for interaction with other ions. Alternatively, it may be that the chemical environment of the Chlamydiae inclusion excludes these potential competing ions, such that there is no selective pressure for greater selectivity. Further studies on Chlamydiae inclusions and the structure-function relationships of the metal-binding sites in YtgA orthologs will resolve these questions.

Collectively, our work demonstrates that *C. trachomatis* YtgA is a cluster A-I SBP with a new variation in the modality of metal-ion coordination (N3O2) as shown for Fe. Although YtgA has been previously reported to be a Fe(III)-specific binding protein, our findings show that YtgA interacts with a range of transition metal ions *in vitro*. Analysis of the stability of protein-metal complexes and whole cell metal accumulation reveal that YtgA is most likely involved in the acquisition of Fe(II), but may also recruit Mn(II) from eukaryotic cells. These findings provide new molecular insights into how *C. trachomatis* acquires Fe from host cells and provide a robust foundation for the development of antimicrobials targeting this crucial

import pathway.

## MATERIALS AND METHODS

### Expression and purification of YtgA

Recombinant YtgA was generated by gene synthesis of *C. trachomatis ytgA* serovar D/UW-3/Cx (Genscript, USA), PCR amplification and ligation-independent cloning using the primers YtgA1F (5' TGGGTGGTGGATTTCCTAACCAGCCGGCAGAT) and Ytg1R (5' TTGGAAGTATAAATTTCCTTCCAGGACCGTGCC) to insert the gene into a C-terminal dodecahistidine tag-containing vector, pCAMcLIC01, and generate pCAMcLIC01-YtgA. Protein expression was performed in *E. coli* Lemo21(DE3), by growing the cells in an autoinducing TB medium (Overnight Express, Merck, USA) using UltraYield Flasks (Thomson Instrument Company, USA), for 18 h at 27 °C, on an Innova 44R shaking incubator at 215 rpm. Cells were harvested, resuspended in 20 mM 4-morpholinepropanesulfonic acid (MOPS) (pH 7.2), 200 mM NaCl, 15 mM imidazole, and 20% glycerol buffer, and disrupted at 30 kPSI by a Constant Systems cell disruptor. The soluble supernatant was then isolated by centrifugation at 4 °C for 60 min at 120,000 × *g*. Purification of YtgA was achieved by a Histrap HP column (GE Healthcare, UK) on an ÄKTA Purifier (GE Healthcare) using a binding buffer containing 20 mM MOPS (pH 7.8), 200 mM NaCl, 10% glycerol, and 15 mM imidazole, and an elution buffer containing 20 mM MOPS (pH 6.6), 200 mM NaCl, 10% glycerol, and 1 M imidazole. The imidazole was removed by buffer exchange on a HiPrep 26/10 Desalting column (GE Healthcare), and sample homogeneity confirmed by size exclusion chromatography on a Superdex 200 10/30 column (GE Healthcare) using an ÄKTA Purifier (GE Healthcare) prior to characterization. Thyroglobulin (669 kDa), apoferritin (443 kDa), β-amylase (200 kDa), alcohol dehydrogenase (150 kDa), albumin (66 kDa) and carbonic anhydrase (29 kDa) were used as molecular weight standards on the Superdex 200 10/30 column, with a blue dextran standard (2 MDa) used to determine the void volume (Sigma-Aldrich, USA).

373

374 **Metal-free YtgA generation and metal content analysis**

375 Recombinant YtgA had the dodecahistidine tag removed by 1 h enzymatic digestion at a ratio
376 of 1:25 by the histidine-tagged 3C human rhinovirus protease, at a cleavage site introduced
377 between YtgA and the tag. The protein was then reverse-purified on a HisTrap HP column (GE
378 Healthcare), with the cleaved protein unable to bind to the column. Removal of the
379 dodecahistidine tag was confirmed by the observed reduction in molecular mass on a 4-12%
380 SDS-PAGE gel and confirmed by immunoblotting. Demetallated (metal-free), tag-free YtgA
381 was prepared by dialyzing the protein (10 ml) in a 10 kDa MWCO membrane (Pierce, USA)
382 against 4 L of sodium acetate buffer, pH 4.0, with 20 mM EDTA, at 25 °C for 24 h. The sample
383 was then dialyzed against 4 L of 20 mM Tris-HCl, pH 7.2, 200 mM NaCl, at 4 °C for 24 h. The
384 sample was then recovered and centrifuged at 120,000 × *g* for 10 min to remove any insoluble
385 material. Demetallated, tag-free YtgA was then desalted into 20 mM MOPS (pH 7.2), 200 mM
386 NaCl, 10% glycerol on a HiPrep 26/10 Desalting column (GE Healthcare). Metal content
387 analysis was performed by inductively coupled plasma-mass spectrometry (ICP-MS). Three
388 micromolar protein was heated at 95 °C for 15 min in 3.5% $HNO_3$. The insoluble material was
389 removed by centrifugation at 18,000 × *g* for 20 min, after which the samples were analysed on
390 an Agilent 7500cx ICP-MS/MS (Adelaide Microscopy, University of Adelaide).

391

392 **YtgA metal binding assays**

393 Metal loading assays were performed on demetallated, tag-cleaved YtgA (20 μM) by mixing
394 with > 10-fold molar excess (200 μM) of $MnSO_4$, $FeSO_4$, $FeCl_3$, $CoCl_2$, $NiCl_2$, $CuSO_4$, $ZnSO_4$,
395 and $CdCl_2$ in a total volume of 2 ml into the binding assay buffer (20 mM MOPS, pH 7.2, 200
396 mM NaCl, 10% glycerol) for 2 h at 4 °C. Metal ion stock solutions for the assays were prepared
397 immediately prior to incubation with YtgA to minimise precipitation and, in the case of $FeSO_4$,

oxidation of Fe(II) to Fe(III). After incubation, unbound metal was removed by buffer exchange on a PD10 column (GE Healthcare) into the binding assay buffer and the protein concentration was determined. Solutions of metal-loaded protein (1.4 – 2 μM) were prepared in 3.5% $HNO_3$ and boiled for 15 min at 95 °C. Samples were then cooled and centrifuged for 20 min at 18,000 × *g*. The supernatant was then analysed by ICP-MS and the protein-to-metal ratio determined.

**Differential scanning fluorimetry**

The differential scanning fluorimetry assays were performed essentially as described previously (35). Briefly, 10 μM demetallated, tag-cleaved YtgA in 20 mM MOPS, pH 7.2, 200 mM NaCl, 10% glycerol, 5 × SYPRO Orange (Life Technologies) was incubated in the presence of 100 μM metal ion and then analysed on a Roche LC480 Real-Time Cycler (Roche Applied Sciences). The samples were pre-incubated for 10 min with the indicated metal ion concentration and then subjected to thermal unfolding from 37 °C to 97 °C at a heating rate of 1 °C per min. Fluorescence data were also collected for buffer only, protein without metal ions, and for each of the metal ions without protein. The fluorescence data were collected by excitation at 470 nm and emission at 570 nm. After subtraction of the background fluorescence from the buffer, the first derivative of the fluorescence data was determined and analysed using Graphpad Prism to determine the inflection point of the melting transition ($T_m$). Data from at least three independent experiments were used to determine the mean $T_m$ (± s.d.) of wild-type YtgA. Statistical significance of the differences in the $T_m$ shifts were determined by a one-way ANOVA using a Tukey post-test.

**Phylogeny**

The sequences of the 32 SBPs included in this study were obtained from the NCBI with the GI

accession numbers: *Bacillus anthracis* MntA, **GI:229264967** (54); *Bacillus subtilis* YcdH, **GI:2415736** (55); *Bacillus subtilis* YclQ, **GI:758317765** (56); *Campylobacter jejuni* ZnuA, **GI:384442496** (57); *Chlamydia trachomatis* YtgA, **GI:73811687** (58); *Escherichia coli* FitE, **GI:190907145** (59); *Escherichia coli* SitA, **GI:84060846** (60); *Escherichia coli* ZnuA, **GI:298380994** (61); *Haemophilus influenzae* FbpA, **GI:1098687** (62); *Haemophilus influenza* ZnuA, **GI:16272089** (63); *Neisseria gonorrhoeae* FbpA **GI:1098687** (64); *Neisseria gonorrhoeae* MntC, **GI:59800624** (65); *Pseudomonas aeruginosa* ZnuA, **GI:15600691** (20); *Sinorhizobium meliloti* SitA, **GI:336034510** (66); *Staphylococcus aureus* HtsA, **GI:537378541** (67),; *Staphylococcus aureus* MntC, **GI:88194402** (68); *Staphylococcus pseudintermedius* SitA, GI:317161313 (34); *Streptococcus pneumoniae* AdcA, **GI:116516060** (69); *Streptococcus pneumoniae* AdcAII, **GI:116515739** (69); *Streptococcus pneumoniae* PiuA, **GI:693295764** (70); *Streptococcus pneumoniae* PsaA, **GI:116515973** (35); *Streptococcus pyogenes* HtsA **GI:114795192** (71); *Streptococcus pyogenes* MtsA, **GI:383493478** (32); *Streptococcus suis* TroA, **GI:386583456** (72); *Synechocystis* MntC, **GI:1653002** (73); *Synechocystis* ZnuA, **GI:38492833** (74); *Treponema pallidum* TroA, **GI:1777933** (31, 75); *Treponema pallidum* ZnuA, **GI:378974662** (75); *Vibrio cholerae* VctP, **GI:469674348** (76); *Yersinia pestis* YfeA, **GI:1245464** (77); *Yersinia pestis* YfuA **GI:913031127** (78); and *Yersinia pestis* ZnuA, **GI:25453364** (79). An alignment of these sequences was created using Clustal Omega and the phylogenetic tree was generated using the neighbour-joining method (80, 81).

### ***C. trachomatis*** **growth and metal content determination**

Whole cell ICP-MS of the isolated *C. trachomatis* was performed essentially as described previously (35). *C. trachomatis* L2 (source ATCC strain 434/Bu) was cultured in McCoy B cells (source: ATCC CRL-1696) at a multiplicity of infection of 5, until 40 h post infection as

448 previously described {Huston, 2008 #3797}. The *C. trachomatis* cells were isolated from host
449 cell debri after cell lysis using ultravist gradient based separation (as per previous protocol
450 {Cunningham, 2013 #3946}).
451
452 **Protein crystallization and structure determination**
453 Purified recombinant, demetallated, tag-free YtgA protein was concentrated to 12 $mg.mL^{-1}$
454 using a centrifugal filter unit (MWCO 10 kDa, Millipore) for crystallization experiments.
455 Equimolar concentration of $FeCl_2$ was added to the protein solution prior to crystallisation. The
456 initial hit was obtained from the PACT sparse matrix screen (82). Following optimization,
457 diffraction-quality Fe-bound YtgA protein crystals were obtained in 22 % (w/v) polyethylene
458 glycol (PEG) 6000, 0.2 M $CaCl_2$, 0.01 M $FeCl_2$ and 0.1 M MES, pH 6.0 after 7 days at 18 °C
459 using the hanging-drop vapour diffusion method. The Fe(II) supplied in the crystallisation
460 solution was likely oxidised to Fe(III) after 3-5 days, based on the colour change of the solution.
461 Prior to data collection, the crystals were soaked in 25 % (v/v) glycerol for cryo-protection and
462 then flash-cooled in liquid nitrogen. Diffraction data were collected at cryogenic temperatures
463 from a single crystal at the Australian Synchrotron MX 1 beamline (83) at X-ray wavelength
464 of 0.954 Å. The data was then processed using XDS (84) and Aimless, CCP4 Suite (85) and
465 the phase information was obtained by molecular replacement by Phaser, Phenix Suite (86)
466 using the crystal structure of pneumococcal PsaA (sequence identity 21 %, **PDB: 1PSZ**) (87)
467 as the search model. The structure model was subsequently created automatically using
468 Phenix.Autobuild (88), and refined iteratively using Phenix.Refine with manual adjustment in
469 COOT (89). Metal ions were modelled based on their peaks in the $mF_O$-$DF_C$ difference density
470 map, together by consideration of the B factors with their coordination ligands, and chemical
471 plausibility. Structure analyses were performed in PyMol (Schrödinger, LLC).
472

## Accession Number

The YtgA atomic coordinates and structure factors were deposited in the Protein Data Bank with accession number **6NSI**.

## ACKNOWLEDGMENTS

We acknowledge the use of the Australian Synchrotron MX beamlines, part of ANSTO, and the facilities, and the scientific and technical assistance of the University of Queensland Remote Operation Crystallization and X-ray Diffraction (UQ-ROCX) Facility and Australian Microscopy & Microanalysis Research Facility at the Centre for Microscopy and Microanalysis, The University of Queensland. This work was supported by the National Health and Medical Research Council (NHMRC) Program Grant 1071659 to B.K. and Project Grant 1122582 to C.A.M. and the Australian Research Council (ARC) Discovery Project Grant DP170102102 to C.A.M. S.L.B. is an NHMRC Early Career Research Fellow (1142695), B.K. is an NHMRC Principal Research Fellow (1110971) and ARC Laureate Fellow (FL180100109), and C.A.M. is an ARC Future Fellow (FT170100006).

## REFERENCES


1. Hentze MW, Muckenthaler MU, Andrews NC. 2004. Balancing acts: molecular control of mammalian iron metabolism. Cell 117:285-97.
2. Frey PA, Reed GH. 2012. The ubiquity of iron. ACS Chem Biol 7:1477-81.
3. Pokorzynski ND, Thompson CC, Carabeo RA. 2017. Ironing out the unconventional mechanisms of iron acquisition and gene regulation in Chlamydia. Front Cell Infect Microbiol 7:394.
4. Oexle H, Gnaiger E, Weiss G. 1999. Iron-dependent changes in cellular energy metabolism: influence on citric acid cycle and oxidative phosphorylation. Biochim Biophys Acta 1413:99-107.
5. Lukianova OA, David SS. 2005. A role for iron-sulfur clusters in DNA repair. Curr Opin Chem Biol 9:145-51.
6. Kim HJ, Khalimonchuk O, Smith PM, Winge DR. 2012. Structure, function, and assembly of heme centers in mitochondrial respiratory complexes. Biochim Biophys Acta 1823:1604-16.
7. West SK. 2004. Trachoma: new assault on an ancient disease. Prog Retin Eye Res 23:381-401.
8. Adderley-Kelly B, Stephens EM. 2005. Chlamydia: A major health threat to adolescents and young adults. ABNF J 16:52-5.
9. Newman L, Rowley J, Vander Hoorn S, Wijesooriya NS, Unemo M, Low N, Stevens G, Gottlieb S, Kiarie J, Temmerman M. 2015. Global estimates of the prevalence and incidence of four curable sexually transmitted infections in 2012 based on systematic review and global reporting. PLoS One 10:e0143304.
10. Abdelrahman YM, Belland RJ. 2005. The chlamydial developmental cycle. FEMS Microbiol Rev 29:949-59.

514 11. Omsland A, Sixt BS, Horn M, Hackstadt T. 2014. Chlamydial metabolism revisited:
515 interspecies metabolic variability and developmental stage-specific physiologic
516 activities. FEMS Microbiol Rev 38:779-801.
517 12. Stephens RS, Kalman S, Lammel C, Fan J, Marathe R, Aravind L, Mitchell W, Olinger
518 L, Tatusov RL, Zhao Q, Koonin EV, Davis RW. 1998. Genome sequence of an obligate
519 intracellular pathogen of humans: *Chlamydia trachomatis*. Science 282:754-9.
520 13. Beatty WL, Morrison RP, Byrne GI. 1994. Persistent chlamydiae: from cell culture to
521 a paradigm for chlamydial pathogenesis. Microbiol Rev 58:686-99.
522 14. Raulston JE. 1997. Response of *Chlamydia trachomatis* serovar E to iron restriction in
523 vitro and evidence for iron-regulated chlamydial proteins. Infect Immun 65:4539-47.
524 15. Caza M, Kronstad JW. 2013. Shared and distinct mechanisms of iron acquisition by
525 bacterial and fungal pathogens of humans. Front Cell Infect Microbiol 3:80.
526 16. Marx JJ. 2002. Iron and infection: competition between host and microbes for a
527 precious element. Best Pract Res Clin Haematol 15:411-26.
528 17. Lau CK, Krewulak KD, Vogel HJ. 2016. Bacterial ferrous iron transport: the Feo
529 system. FEMS Microbiol Rev 40:273-98.
530 18. Perry RD, Mier I, Jr., Fetherston JD. 2007. Roles of the Yfe and Feo transporters of
531 Yersinia pestis in iron uptake and intracellular growth. Biometals 20:699-703.
532 19. Miller JD, Sal MS, Schell M, Whittimore JD, Raulston JE. 2009. *Chlamydia*
533 *trachomatis* YtgA is an iron-binding periplasmic protein induced by iron restriction.
534 Microbiology 155:2884-94.
535 20. Pederick VG, Eijkelkamp BA, Begg SL, Ween MP, McAllister LJ, Paton JC, McDevitt
536 CA. 2015. ZnuA and zinc homeostasis in *Pseudomonas aeruginosa*. Sci Rep 5:13139.
537 21. Plumptre CD, Eijkelkamp BA, Morey JR, Behr F, Couñago RM, Ogunniyi AD, Kobe
538 B, O'Mara ML, Paton JC, McDevitt CA. 2014. AdcA and AdcAII employ distinct zinc

539 acquisition mechanisms and contribute additively to zinc homeostasis in *Streptococcus*
540 *pneumoniae*. Mol Microbiol 91:834-51.
541 22. Petersen TN, Brunak S, von Heijne G, Nielsen H. 2011. SignalP 4.0: discriminating
542 signal peptides from transmembrane regions. Nat Methods 8:785-6.
543 23. Begg SL, Eijkelkamp BA, Luo Z, Couñago RM, Morey JR, Maher MJ, Ong CL,
544 McEwan AG, Kobe B, O'Mara ML, Paton JC, McDevitt CA. 2015. Dysregulation of
545 transition metal ion homeostasis is the molecular basis for cadmium toxicity in
546 *Streptococcus pneumoniae*. Nat Commun 6:6418.
547 24. Martell AE. 1977. Critical Stability Constants, vol 3. Plenum, New York.
548 25. Eijkelkamp BA, McDevitt CA, Kitten T. 2015. Manganese uptake and streptococcal
549 virulence. Biometals 28:491-508.
550 26. Couñago RM, McDevitt CA, Ween MP, Kobe B. 2012. Prokaryotic substrate-binding
551 proteins as targets for antimicrobial therapies. Curr Drug Targets 13:1400-10.
552 27. Radka CD, DeLucas LJ, Wilson LS, Lawrenz MB, Perry RD, Aller SG. 2017. Crystal
553 structure of *Yersinia pestis* virulence factor YfeA reveals two polyspecific metal-
554 binding sites. Acta Crystallogr D Struct Biol 73:557-572.
555 28. Trakhanov S, Vyas NK, Luecke H, Kristensen DM, Ma J, Quiocho FA. 2005. Ligand-
556 free and -bound structures of the binding protein (LivJ) of the Escherichia coli ABC
557 leucine/isoleucine/valine transport system: trajectory and dynamics of the interdomain
558 rotation and ligand specificity. Biochemistry 44:6597-608.
559 29. Felder CB, Graul RC, Lee AY, Merkle HP, Sadee W. 1999. The Venus flytrap of
560 periplasmic binding proteins: an ancient protein module present in multiple drug
561 receptors. AAPS PharmSci 1:E2.

562 30. Couñago RM, Ween MP, Begg SL, Bajaj M, Zuegg J, O'Mara ML, Cooper MA,
563 McEwan AG, Paton JC, Kobe B, McDevitt CA. 2014. Imperfect coordination
564 chemistry facilitates metal ion release in the Psa permease. Nat Chem Biol 10:35-41.
565 31. Lee YH, Deka RK, Norgard MV, Radolf JD, Hasemann CA. 1999. *Treponema*
566 *pallidum* TroA is a periplasmic zinc-binding protein with a helical backbone. Nat Struct
567 Biol 6:628-33.
568 32. Sun X, Baker HM, Ge R, Sun H, He QY, Baker EN. 2009. Crystal structure and metal
569 binding properties of the lipoprotein MtsA, responsible for iron transport in
570 *Streptococcus pyogenes*. Biochemistry 48:6184-90.
571 33. Gribenko A, Mosyak L, Ghosh S, Parris K, Svenson K, Moran J, Chu L, Li S, Liu T,
572 Woods VL, Jr., Jansen KU, Green BA, Anderson AS, Matsuka YV. 2013. Three-
573 dimensional structure and biophysical characterization of *Staphylococcus aureus* cell
574 surface antigen-manganese transporter MntC. J Mol Biol 425:3429-45.
575 34. Abate F, Malito E, Cozzi R, Lo Surdo P, Maione D, Bottomley MJ. 2014. Apo, $Zn^{2+}$-
576 bound and $Mn^{2+}$-bound structures reveal ligand-binding properties of SitA from the
577 pathogen *Staphylococcus pseudintermedius*. Biosci Rep 34:e00154.
578 35. McDevitt CA, Ogunniyi AD, Valkov E, Lawrence MC, Kobe B, McEwan AG, Paton
579 JC. 2011. A molecular mechanism for bacterial susceptibility to zinc. PLoS Pathog
580 7:e1002357.
581 36. Yatsunyk LA, Easton JA, Kim LR, Sugarbaker SA, Bennett B, Breece RM, Vorontsov,
582 II, Tierney DL, Crowder MW, Rosenzweig AC. 2008. Structure and metal binding
583 properties of ZnuA, a periplasmic zinc transporter from *Escherichia coli*. J Biol Inorg
584 Chem 13:271-88.

585 37. Loisel E, Jacquamet L, Serre L, Bauvois C, Ferrer JL, Vernet T, Di Guilmi AM,
586 Durmort C. 2008. AdcAII, a new pneumococcal Zn-binding protein homologous with
587 ABC transporters: biochemical and structural analysis. J Mol Biol 381:594-606.
588 38. Thompson CC, Nicod SS, Malcolm DS, Grieshaber SS, Carabeo RA. 2012. Cleavage
589 of a putative metal permease in *Chlamydia trachomatis* yields an iron-dependent
590 transcriptional repressor. Proc Natl Acad Sci U S A 109:10546-51.
591 39. Garmer DR, Gresh N. 1994. A comprehensie energy component analysis of the
592 interaction of hard and soft dications with biological ligands. J Am Chem Soc
593 116:3556-3567.
594 40. Dudev T, Lim C. 2008. Metal binding affinity and selectivity in metalloproteins:
595 insights from computational studies. Annu Rev Biophys 37:97-116.
596 41. Ilari A, Alaleona F, Petrarca P, Battistoni A, Chiancone E. 2011. The X-ray structure
597 of the zinc transporter ZnuA from *Salmonella enterica* discloses a unique triad of zinc-
598 coordinating histidines. J Mol Biol 409:630-41.
599 42. de Boer M, Gouridis G, Vietrov R, Begg SL, Schuurman-Wolters GK, Husada F,
600 Eleftheriadis N, Poolman B, McDevitt CA, Cordes T. 2019. Conformational and
601 dynamic plasticity in substrate-binding proteins underlies selective transport in ABC
602 importers. Elife 8.
603 43. Ba LA, Doering M, Burkholz T, Jacob C. 2009. Metal trafficking: from maintaining
604 the metal homeostasis to future drug design. Metallomics 1:292-311.
605 44. Williams RJ. 1982. Free manganese (II) and iron (II) cations can act as intracellular cell
606 controls. FEBS Lett 140:3-10.
607 45. Maret W. 2015. Analyzing free zinc(II) ion concentrations in cell biology with
608 fluorescent chelating molecules. Metallomics 7:202-11.

609 46. van Ooij C, Apodaca G, Engel J. 1997. Characterization of the *Chlamydia trachomatis*
610 vacuole and its interaction with the host endocytic pathway in HeLa cells. Infect Immun
611 65:758-66.
612 47. Ouellette SP, Carabeo RA. 2010. A functional slow recycling pathway of transferrin is
613 required for growth of Chlamydia. Front Microbiol 1:112.
614 48. Pan X, Tamilselvam B, Hansen EJ, Daefler S. 2010. Modulation of iron homeostasis in
615 macrophages by bacterial intracellular pathogens. BMC Microbiol 10:64.
616 49. Humphrys MS, Creasy T, Sun Y, Shetty AC, Chibucos MC, Drabek EF, Fraser CM,
617 Farooq U, Sengamalay N, Ott S, Shou H, Bavoil PM, Mahurkar A, Myers GS. 2013.
618 Simultaneous transcriptional profiling of bacteria and their host cells. PLoS One
619 8:e80597.
620 50. Scidmore MA, Fischer ER, Hackstadt T. 1996. Sphingolipids and glycoproteins are
621 differentially trafficked to the *Chlamydia trachomatis* inclusion. J Cell Biol 134:363-
622 74.
623 51. Al-Younes HM, Rudel T, Brinkmann V, Szczepek AJ, Meyer TF. 2001. Low iron
624 availability modulates the course of *Chlamydia pneumoniae* infection. Cell Microbiol
625 3:427-37.
626 52. Matsumoto A, Bessho H, Uehira K, Suda T. 1991. Morphological studies of the
627 association of mitochondria with chlamydial inclusions and the fusion of chlamydial
628 inclusions. J Electron Microsc (Tokyo) 40:356-63.
629 53. Al-Younes HM, Brinkmann V, Meyer TF. 2004. Interaction of *Chlamydia trachomatis*
630 serovar L2 with the host autophagic pathway. Infect Immun 72:4751-62.
631 54. Gat O, Mendelson I, Chitlaru T, Ariel N, Altboum Z, Levy H, Weiss S, Grosfeld H,
632 Cohen S, Shafferman A. 2005. The solute-binding component of a putative Mn(II) ABC

633 transporter (MntA) is a novel *Bacillus anthracis* virulence determinant. Mol Microbiol
634 58:533-51.
635 55. Gaballa A, Helmann JD. 1998. Identification of a zinc-specific metalloregulatory
636 protein, Zur, controlling zinc transport operons in *Bacillus subtilis*. J Bacteriol
637 180:5815-21.
638 56. Zawadzka AM, Kim Y, Maltseva N, Nichiporuk R, Fan Y, Joachimiak A, Raymond
639 KN. 2009. Characterization of a *Bacillus subtilis* transporter for petrobactin, an anthrax
640 stealth siderophore. Proc Natl Acad Sci U S A 106:21854-9.
641 57. Davis LM, Kakuda T, DiRita VJ. 2009. A *Campylobacter jejuni znuA* orthologue is
642 essential for growth in low-zinc environments and chick colonization. J Bacteriol
643 191:1631-40.
644 58. Raulston JE, Miller JD, Davis CH, Schell M, Baldwin A, Ferguson K, Lane H. 2007.
645 Identification of an iron-responsive protein that is antigenic in patients with *Chlamydia*
646 *trachomatis* genital infections. FEMS Immunol Med Microbiol 51:569-76.
647 59. Shi R, Proteau A, Wagner J, Cui Q, Purisima EO, Matte A, Cygler M. 2009. Trapping
648 open and closed forms of FitE: a group III periplasmic binding protein. Proteins 75:598-
649 609.
650 60. Sabri M, Leveille S, Dozois CM. 2006. A SitABCD homologue from an avian
651 pathogenic *Escherichia coli* strain mediates transport of iron and manganese and
652 resistance to hydrogen peroxide. Microbiology 152:745-58.
653 61. Patzer SI, Hantke K. 1998. The ZnuABC high-affinity zinc uptake system and its
654 regulator Zur in *Escherichia coli*. Mol Microbiol 28:1199-210.
655 62. Khambati HK, Moraes TF, Singh J, Shouldice SR, Yu RH, Schryvers AB. 2010. The
656 role of vicinal tyrosine residues in the function of *Haemophilus influenzae* ferric-
657 binding protein A. Biochem J 432:57-64.

658 63. Lu D, Boyd B, Lingwood CA. 1997. Identification of the key protein for zinc uptake in
659 *Hemophilus influenzae*. J Biol Chem 272:29033-8.
660 64. Chen W, Ye D, Wang H, Lin D, Huang J, Sun H, Zhong W. 2013. Binding of oxo-Cu2
661 clusters to ferric ion-binding protein A from *Neisseria gonorrhoeae*: a structural
662 insight. Metallomics 5:1430-9.
663 65. Lim KH, Jones CE, vanden Hoven RN, Edwards JL, Falsetta ML, Apicella MA,
664 Jennings MP, McEwan AG. 2008. Metal binding specificity of the MntABC permease
665 of *Neisseria gonorrhoeae* and its influence on bacterial growth and interaction with
666 cervical epithelial cells. Infect Immun 76:3569-76.
667 66. Davies BW, Walker GC. 2007. Disruption of *sitA* compromises *Sinorhizobium meliloti*
668 for manganese uptake required for protection against oxidative stress. J Bacteriol
669 189:2101-9.
670 67. Grigg JC, Cooper JD, Cheung J, Heinrichs DE, Murphy ME. 2010. The *Staphylococcus*
671 *aureus* siderophore receptor HtsA undergoes localized conformational changes to
672 enclose staphyloferrin A in an arginine-rich binding pocket. J Biol Chem 285:11162-
673 71.
674 68. Horsburgh MJ, Wharton SJ, Cox AG, Ingham E, Peacock S, Foster SJ. 2002. MntR
675 modulates expression of the PerR regulon and superoxide resistance in *Staphylococcus*
676 *aureus* through control of manganese uptake. Mol Microbiol 44:1269-86.
677 69. Bayle L, Chimalapati S, Schoehn G, Brown J, Vernet T, Durmort C. 2011. Zinc uptake
678 by *Streptococcus pneumoniae* depends on both AdcA and AdcAII and is essential for
679 normal bacterial morphology and virulence. Mol Microbiol 82:904-16.
680 70. Tai SS, Yu C, Lee JK. 2003. A solute binding protein of *Streptococcus pneumoniae*
681 iron transport. FEMS Microbiol Lett 220:303-8.

682 71. Nygaard TK, Blouin GC, Liu M, Fukumura M, Olson JS, Fabian M, Dooley DM, Lei
683 B. 2006. The mechanism of direct heme transfer from the streptococcal cell surface
684 protein Shp to HtsA of the HtsABC transporter. J Biol Chem 281:20761-71.
685 72. Zheng B, Zhang Q, Gao J, Han H, Li M, Zhang J, Qi J, Yan J, Gao GF. 2011. Insight
686 into the interaction of metal ions with TroA from *Streptococcus suis*. PLoS One
687 6:e19510.
688 73. Adir N, Rukhman V, Brumshtein B, Anati R. 2002. Preliminary X-ray crystallographic
689 analysis of a soluble form of MntC, a periplasmic manganese-binding component of an
690 ABC-type Mn transporter from *Synechocystis* sp. PCC 6803. Acta Crystallogr D Biol
691 Crystallogr 58:1476-8.
692 74. Banerjee S, Wei B, Bhattacharyya-Pakrasi M, Pakrasi HB, Smith TJ. 2003. Structural
693 determinants of metal specificity in the zinc transport protein ZnuA from *Synechocystis*
694 6803. J Mol Biol 333:1061-9.
695 75. Desrosiers DC, Sun YC, Zaidi AA, Eggers CH, Cox DL, Radolf JD. 2007. The general
696 transition metal (Tro) and $Zn^{2+}$ (Znu) transporters in *Treponema pallidum*: analysis of
697 metal specificities and expression profiles. Mol Microbiol 65:137-52.
698 76. Liu X, Du Q, Wang Z, Liu S, Li N, Chen Y, Zhu C, Zhu D, Wei T, Huang Y, Xu S, Gu
699 L. 2012. Crystal structure of periplasmic catecholate-siderophore binding protein VctP
700 from *Vibrio cholerae* at 1.7 Å resolution. FEBS Lett 586:1240-4.
701 77. Bearden SW, Staggs TM, Perry RD. 1998. An ABC transporter system of *Yersinia*
702 *pestis* allows utilization of chelated iron by *Escherichia coli* SAB11. J Bacteriol
703 180:1135-47.
704 78. Gong S, Bearden SW, Geoffroy VA, Fetherston JD, Perry RD. 2001. Characterization
705 of the Yersinia pestis Yfu ABC inorganic iron transport system. Infect Immun 69:2829-
706 37.

79. Bobrov AG, Kirillina O, Fetherston JD, Miller MC, Burlison JA, Perry RD. 2014. The *Yersinia pestis* siderophore, yersiniabactin, and the ZnuABC system both contribute to zinc acquisition and the development of lethal septicaemic plague in mice. Mol Microbiol 93:759-75.

80. Larkin MA, Blackshields G, Brown NP, Chenna R, McGettigan PA, McWilliam H, Valentin F, Wallace IM, Wilm A, Lopez R, Thompson JD, Gibson TJ, Higgins DG. 2007. Clustal W and Clustal X version 2.0. Bioinformatics 23:2947-8.

81. Sievers F, Wilm A, Dineen D, Gibson TJ, Karplus K, Li W, Lopez R, McWilliam H, Remmert M, Soding J, Thompson JD, Higgins DG. 2011. Fast, scalable generation of high-quality protein multiple sequence alignments using Clustal Omega. Mol Syst Biol 7:539.

82. Newman J, Egan D, Walter TS, Meged R, Berry I, Ben Jelloul M, Sussman JL, Stuart DI, Perrakis A. 2005. Towards rationalization of crystallization screening for small- to medium-sized academic laboratories: the PACT/JCSG+ strategy. Acta Crystallogr D Biol Crystallogr 61:1426-31.

83. Cowieson NP, Aragao D, Clift M, Ericsson DJ, Gee C, Harrop SJ, Mudie N, Panjikar S, Price JR, Riboldi-Tunnicliffe A, Williamson R, Caradoc-Davies T. 2015. MX1: a bending-magnet crystallography beamline serving both chemical and macromolecular crystallography communities at the Australian Synchrotron. J Synchrotron Radiat 22:187-90.

84. Kabsch W. 2010. Xds. Acta Crystallogr D Biol Crystallogr 66:125-32.

85. CCP4. 1994. The CCP4 suite: programs for protein crystallography. Acta Crystallogr D Biol Crystallogr 50:760-3.

86. McCoy AJ. 2007. Solving structures of protein complexes by molecular replacement with Phaser. Acta Crystallogr D Biol Crystallogr 63:32-41.

87. Lawrence MC, Pilling PA, Epa VC, Berry AM, Ogunniyi AD, Paton JC. 1998. The crystal structure of pneumococcal surface antigen PsaA reveals a metal-binding site and a novel structure for a putative ABC-type binding protein. Structure 6:1553-61.
88. Terwilliger TC, Grosse-Kunstleve RW, Afonine PV, Moriarty NW, Zwart PH, Hung LW, Read RJ, Adams PD. 2008. Iterative model building, structure refinement and density modification with the PHENIX AutoBuild wizard. Acta Crystallogr D Biol Crystallogr 64:61-9.
89. Emsley P, Lohkamp B, Scott WG, Cowtan K. 2010. Features and development of Coot. Acta Crystallogr D Biol Crystallogr 66:486-501.

743 **TABLES**

744 **Table 1. Effect of divalent cations on the melting temperature of YtgA**

| Protein [a] | $T_m$ (°C) [b] | $\Delta T_m$ (°C) |
|---|---|---|
| Metal-free YtgA | 50.52 ± 0.87 | - |
| Mg(II)-YtgA | 49.65 ± 2.83 | -1.0 |
| Ca(II)-YtgA | 48.97 ± 3.05 | -1.0 |
| Mn(II)-YtgA | 58.82 ± 1.51 | +7.7 [c] |
| Fe(II)-YtgA | 61.94 ± 0.95 | +9.8 [c] |
| Fe(III)-YtgA | 51.38 ± 0.61 | +0.7 |
| Co(II)-YtgA | 76.01 ± 1.13 | +25.4 [c] |
| Ni(II)-YtgA | 63.26 ± 1.55 | +12.6 [c] |
| Cu(II)-YtgA | n.d.[d] | - |
| Zn(II)-YtgA | 71.59 ± 1.59 | +16.6 [c] |
| Cd(II)-YtgA | 71.83 ± 0.59 | +19.9 [c] |

745

746 [a.] Melting curves for cations that induce a $T_m$ shift are shown in Fig. 4.

747 [b.] Values shown represent the average and standard error of the mean from at least 3

748 independent measurements.

749 [c.] Statistically significant difference to metal-free protein *Tm* (one-way ANOVA with Tukey

750 post-test).

751 [d.] not determined (n.d.)

752

753 **Table 2. Crystallographic data collection and refinement statistics**

| | |
|---|---|
| **Data Collection** | |
| Wavelength (Å) | 0.954 |
| Resolution range (Å) | 19.08-2.00 (2.07-2.00) |
| Space group | *C* 1 2 1 |
| a, b, c (Å) | 47.8, 61.1, 105.5 |
| α, β, γ (°) | 90.0, 96.9, 90.0 |
| Completeness (%) | 100.0 (99.9) |
| $R_{merge}$ | 0.09 (1.00) |
| $R_{pim}$ | 0.04 (0.39) |
| CC(1/2) | 0.99 (0.69) |
| $< I / \sigma(I) >$ | 16.51 (2.03) |
| Multiplicity | 7.3 (7.2) |
| No. unique reflections | 20476 (2001) |
| **Refinement** | |
| $R_{work}$/ $R_{free}$ (%) | 17.9/22.5 |
| **No. of atoms** | |
| Protein | 2324 |
| Ligand/ion | 4 |

| | |
|---|---|
| Water | 208 |
| **Average B-factors (Å$^2$)** | |
| Protein | 38.9 |
| Ligand/ion | 40.8 |
| Waters | 42.1 |
| **Rmsd** | |
| Bond lengths (Å) | 0.01 |
| Bond angles (°) | 0.89 |

754

755 Values in parentheses correspond to the highest resolution shell.

$R_{merge} = \sum_{hkl}\sum_j |I_{hkl,j} - < I_{hkl} > |/(\sum_{hkl}\sum_j I_{hkl,j})$

$R_{pim} = \sum_{hkl}\sqrt{n/(n-1)}\sum_j |I_{hkl,j} - < I_{hkl} > |/(\sum_{hkl}\sum_j I_{hkl,j})$

$R_{work}$ / $R_{free} = \sum_{hkl}\left|F_{hkl}^{obs} - F_{hkl}^{calc}\right|/(\sum_{hkl}F_{hkl}^{obs})$

$R_{free}$ was calculated using randomly chosen 5 % fraction of data that was excluded from refinement.

756

757

**Table 3. Sequence and structural similarities of YtgA with homologous SBPs.**

| Protein | RMSD (Å) | Sequence identity (%) | Number of $C_\alpha$ aligned | PDB ID |
|---|---|---|---|---|
| *T. pallidium* TroA | 1.00 | 24.2 | 261 | 1TOA |
| *S. pyogenes* MtsA | 1.15 | 22.6 | 255 | 3HH8 |
| *Y. pestis* YfeA | 1.06 | 21.9 | 250 | 5UY4 |
| *S. pseudintermedius* SitA | 1.34 | 18.7 | 264 | 4OXR |
| *S. pneumoniae* PsaA | 1.29 | 22.8 | 256 | 3ZTT |
| *E. coli* ZnuA | 1.85 | 14.7 | 179 | 2PS0 |
| *S. aureus* MntC | 1.07 | 19.6 | 226 | 4K3V |
| *S. pneumoniae* AdcAII | 1.65 | 18.8 | 239 | 3CX3 |

## FIGURE LEGENDS

**Figure 1. Phylogenetic analysis of *C. trachomatis* YtgA.** (**a**) YtgA was aligned to the amino-acid sequences of 31 other characterised cluster A-I and A-II SBPs using Clustal Omega. The resulting tree, generated using the neighbour-joining method, displays 4 main clades comprising the cluster A-II SBPs (green) and the cluster A-I SBPs subgroups associated with zinc binding (red); manganese and / or iron binding (blue); and a clade of SBPs with broad (Mn, Zn and Fe) substrate specificity (shaded purple). *C. trachomatis* YtgA clusters with the latter group. (**b**) Sequence alignment of *C. trachomatis* YtgA, and representative cluster A-I SBPs from the other clades. Ctr_YtgA, *C. trachomatis* YtgA (**GI:73811687**); ZnuA_Eco, *E. coli* ZnuA (**GI:635897169**); AdcA_Spn, *S. pneumoniae* AdcA (**GI:116516060**); TroA_Tpa, *T. palladium* (**GI:504108253**); TroA_Sps, *S. suis* (**GI: 386583456**); MntC_Sau, *S. aureus* MntC (**GI:88194402**); PsaA_Spn, *S. pneumoniae* PsaA (**GI:116515973**). Amino acid sequences are coloured according to the clustering in (a) with the region enriched for acidic amino acids in zinc-specific SBPs highlighted in yellow and residue numbers shown.

**Figure 2. Sequence comparison and secondary structure prediction of chlamydial YtgA proteins.** Sequences were aligned using Clustal Omega, using full length YtgA amino acid sequences from *C. trachomatis* (**GI:73811687**), *C. muridarum* (**GI:497916051**), *C. suis* (**GI:737424856**), *C. psittaci* (**GI:493386917**), and *C. pneumoniae* (**GI:33236198**). Metal-coordinating residues are coloured in red. Elements of secondary structure (red cylinder: α-helix; yellow arrow: β-strand) were assigned to the sequences based on the crystal structure of *C. trachomatis* YtgA resolved in this study. Numbers of the amino acids are indicated at the end of each line.

**Figure 3. Purification and biochemical characterisation of YtgA.** (**a**) Determination of the apparent molecular mass of tag-free YtgA by size exclusion chromatography on a Superdex 200 10/300 column. Inset is the linear regression of the protein molecular weight standards used to calibrate the column. YtgA eluted with a monomeric molecular mass of 36.2 kDa. (**b**) Coomassie blue-stained 12.5% SDS polyacrylamide gel showing (arrow) purified YtgA.

**Figure 4. DSF analyses of YtgA.** Thermostability of demetallated, tag-free YtgA (dashed line) and metal-incubated (solid line) YtgA with a 10-fold concentration of the shown transition metal ion (**a**) Mn(II), (**b**) Fe(II), (**c**) Fe(III), (**d**) Co(II), (**e**) Ni(II), (**f**) Zn(II), and (**g**) Cd(II) or (**h**) a 100-fold concentration of Fe(III). Data are presented as the first derivative of the SYPRO Orange fluorescence with the inflection point value ($T_m$) of the solid line shown.

**Figure 5. Transition metal-ion interaction with YtgA.** *In vitro* metal-binding experiments with demetallated, tag-free YtgA and transition metal ions as shown and analysed by ICP-MS. The molar ratio of metal ion-to-YtgA was determined and data correspond to mean values (± s.d.) of at least 4 independent biological experiments. Statistical significance of the differences relative to demetallated, tag-free YtgA was determined by a one-way ANOVA with Sidak post-test (n.s. not significant; **** P value < 0.0001).

**Figure 6. Cellular metal accumulation of *C. trachomatis*.** Total cellular metal-ion accumulation of *C. trachomatis* elementary bodies represented as the mean (± s.d.) concentration of ions per cell, determined as μg metal.$g^{-1}$ cells (dry weight). The values are from at two independent biological experiments. Metal-ions assessed were Mn, Fe, Co, Ni, Cu, and Zn. (b.d. corresponds to 'below detection').

**Figure 7. Crystal structure of Fe(III)-bound YtgA.** (**a**) "Side" and (**b**) "top" views of the cartoon illustration of Fe-bound, tag-free YtgA in the closed conformation. The protein consists of N-terminal (green) and C-terminal (red) globular domains with a domain-linking helix (cyan). All the secondary structures are labelled with black text. The metal-binding site situates at the interface between the two domains. The bound Fe atom is shown by a black sphere and its coordinating residues are in stick representation. (**c**) Surface "side" view of YtgA crystal structure. The bound Fe (black sphere) is completely buried in the protein. The N-terminal, C-terminal and the domain-linking helix are shown in green, red and cyan, respectively. (**d**) The metal-binding site of YtgA. The bound Fe (black sphere) is coordinated by three nitrogen atoms from His75, His141 and His207, respectively, and two oxygen atoms from Asp299 in a distorted trigonal bipyramidal geometry. The metal-coordinating residues are shown in stick and ball representation and the coordination bonds are represented by dashed lines. The $2F_o$-$F_c$ electron density map (blue mesh) shown is contoured at 1.5σ.

**Figure 8. Structural comparison of YtgA with structural homologs.** (**a**) "Side" and (**b**) "top" views of structural superimposition of selected crystal structures. Green: *C. trachomatis* YtgA; cyan: *T. pallidum* TroA (PDB: 1TOA); orange: *S. pneumoniae* AdcAII (PDB: 3CX3); magenta: *S. pyogenes* MtsA (PDB: 3HH8); yellow: *Y. pestis* YfeA (PDB: 5UY4); light blue: *S. aureus* MntC (PDB: 4K3V); black: *S. pneumoniae* PsaA (PDB: 3ZTT). Bound metal ions are shown by spheres and their coordinating residues in stick representation. The unique α-helices of YtgA are labelled. The structures were superimposed using the Cα atoms in PyMol with comparisons of the metal-binding sites to YtgA shown for: (**c**) Zn(II)-binding SBPs, (**d**) Fe-binding SBPs, and (**e**) Mn(II)-binding SBPs. The metal-coordinating residues are labelled based on YtgA in (c). Orientations of the view in (d) and (e) are consistent with the view in (c).

834 Bound metal ions (spheres) and their coordinating atoms (small spheres) from the respective
835 residues (sticks) are shown.
836
837

## FIGURES

### Figure 1

(a)

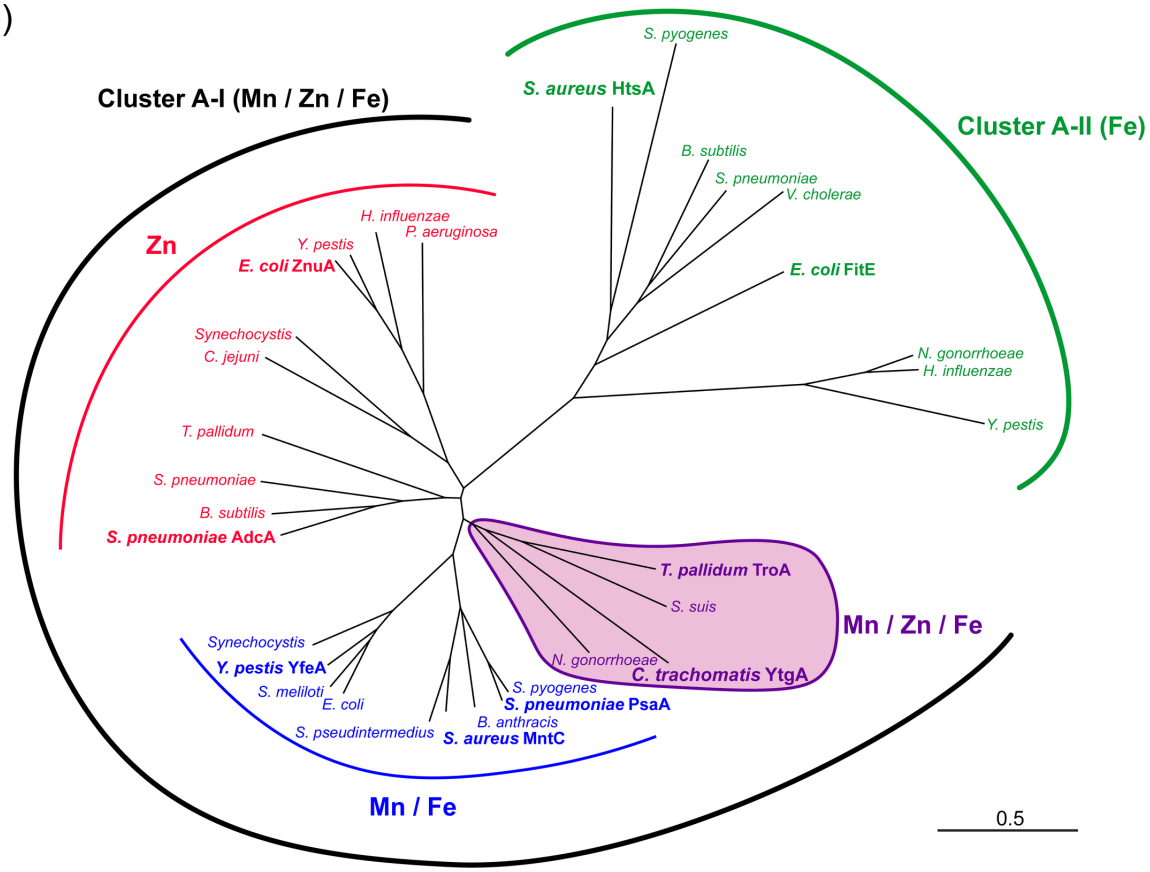


(b)

```
YtgA_Ctr  ASL-RKHLEGNPK------VVDLGQRLLN--------K---NCFDLLSEEGFPDPHIWTD 145
ZnuA_Eco  MQKPVSKLPGAKQVTI-AQLEDVKPLLMKSIHGDDDDHDHAEKSDEDHHHGDFNMHLWLS 147
AdcA_Spn  --TWVPKLLDTLDKKKVKTIKATGDMLLL-PGGEEEEGD--HDHGEEGHHHEFDPHVWLS 144
TroA_Tpa  MGEVFSKLRGSRL------VVAVSE-------TIPV------SQRLSLEEAEFDPHVWFD 137
TroA_Sps  MVEALEKTGV----------AVSK-------NFNA-KD--LNTMDEDGEEIVDPHFWFS 108
MntC_Sau  --RWFEQFLGNVKDVP---SVVLTE-------GIEP-I----PIADGPYTDKPNPHAWMS 158
PsaA_Spn  GNAWFTKLVENAKKTENKDYFAVSD-------GVDV-I----YLEGQNEKGKEDPHAWLN 143
```

845 **Figure 2**

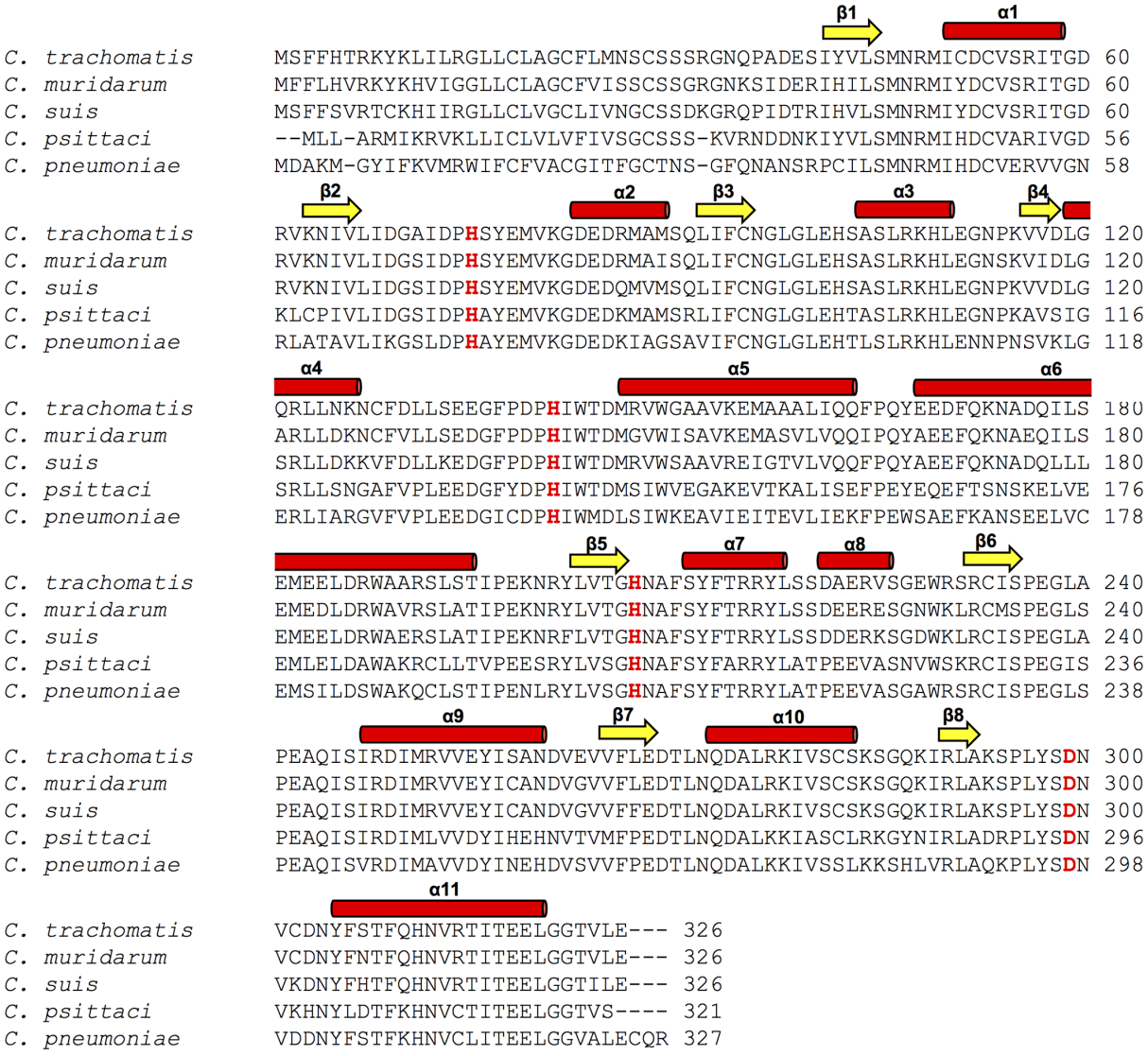


847

848 **Figure 3**

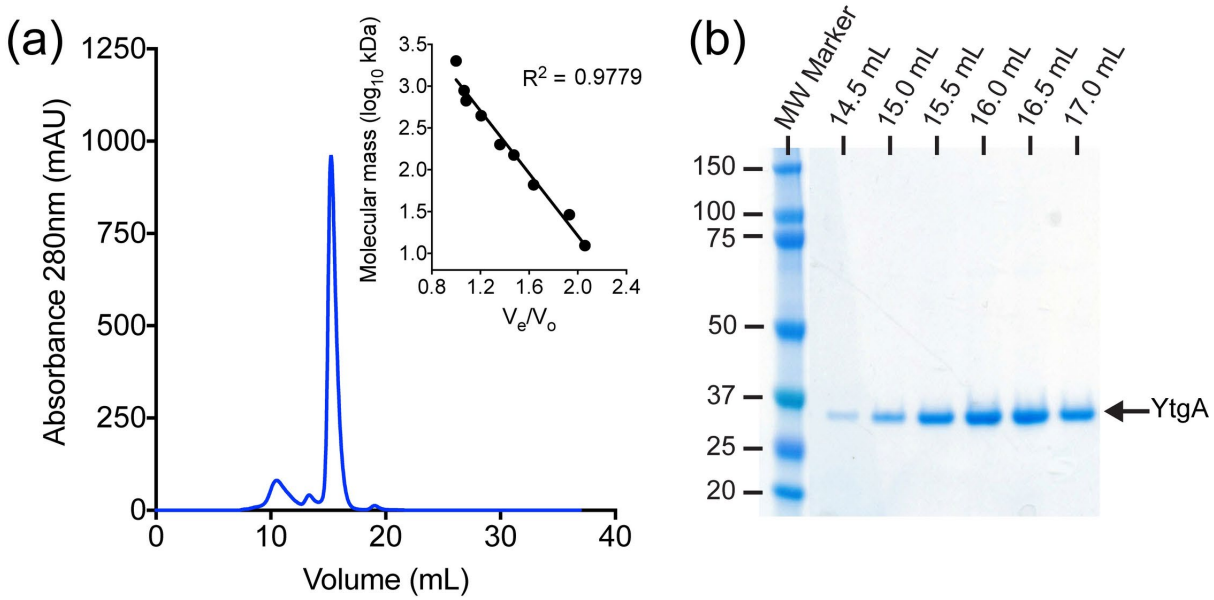


849

850

851

852 **Figure 4**

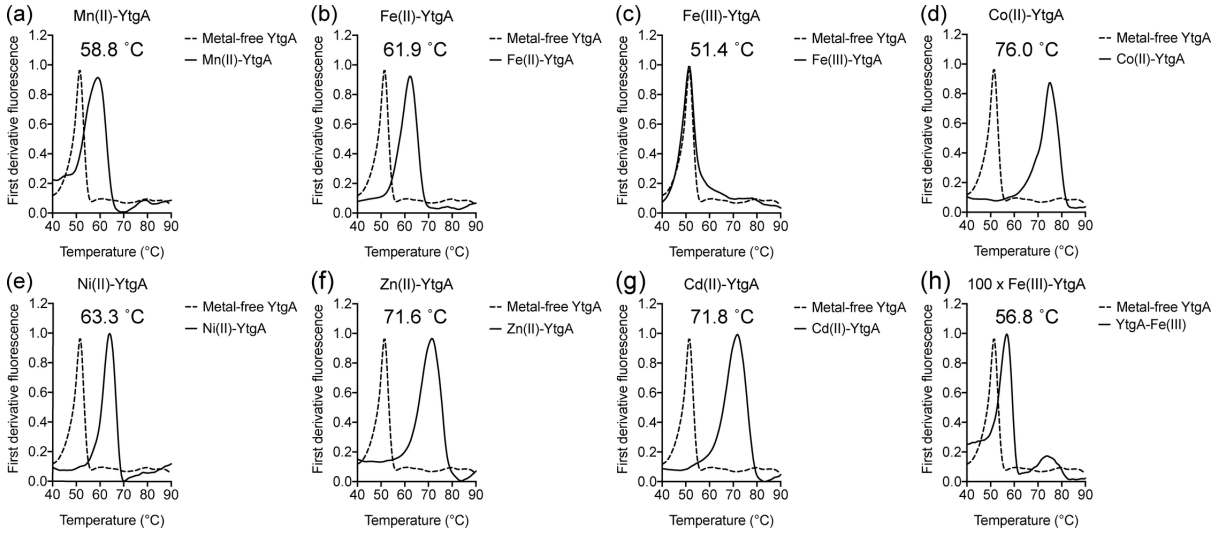


853

854

855

856

**Figure 5**

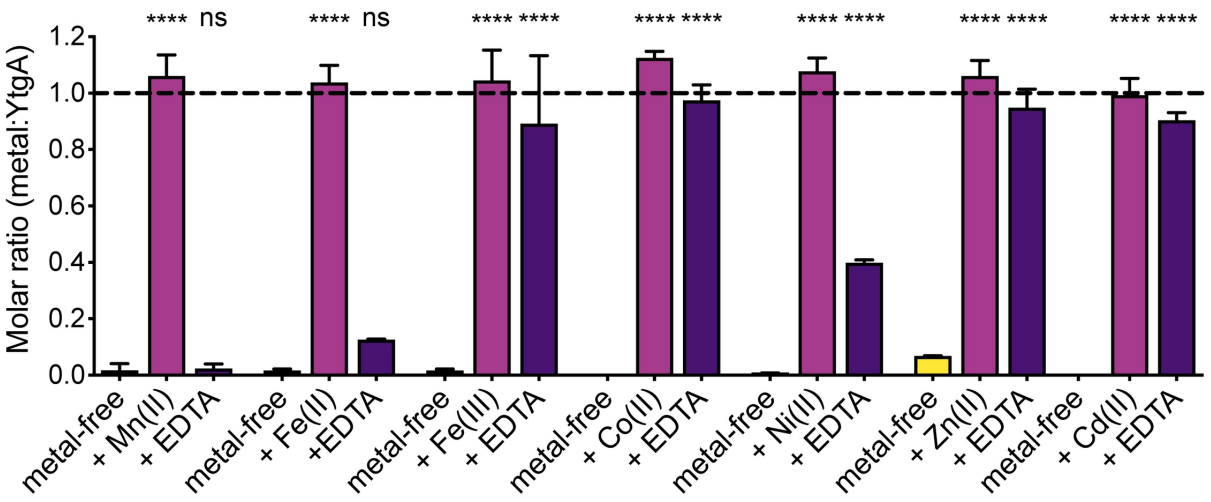
Molar ratio (metal:YtgA)
1.2
1.0
0.8
0.6
0.4
0.2
0.0
**** ns
**** ns
**** ****
**** ****
**** ****
**** ****
**** ****
metal-free
+ Mn(II)
+ EDTA
metal-free
+ Fe(II)
+EDTA
metal-free
+ Fe(III)
+ EDTA
metal-free
+ Co(II)
+ EDTA
metal-free
+ Ni(II)
+ EDTA
metal-free
+ Zn(II)
+ EDTA
metal-free
+ Cd(II)
+ EDTA

861 **Figure 6**

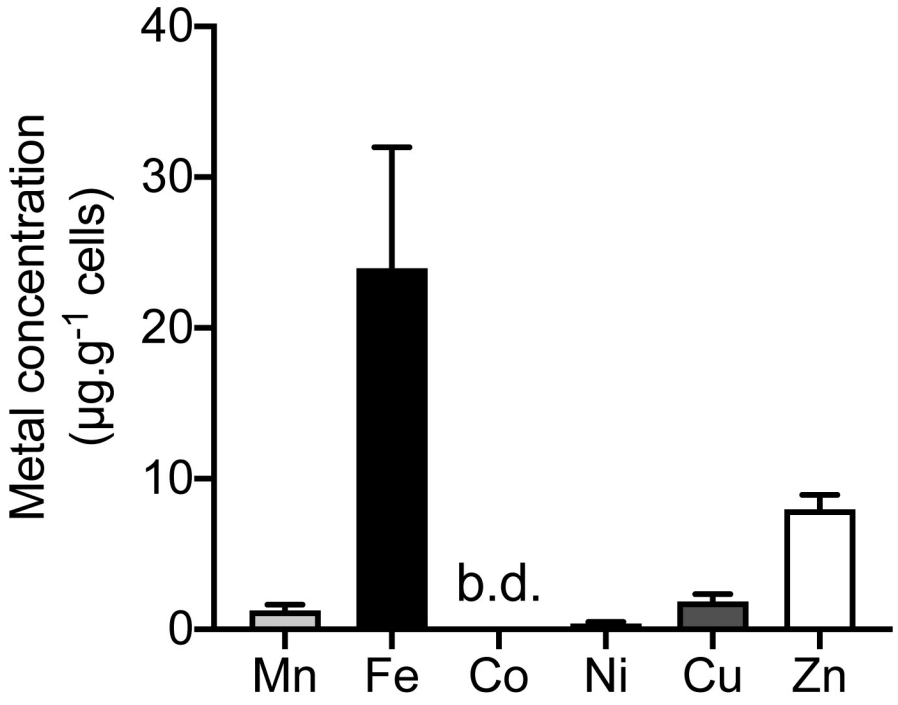


862

863

864

865 **Figure 7**

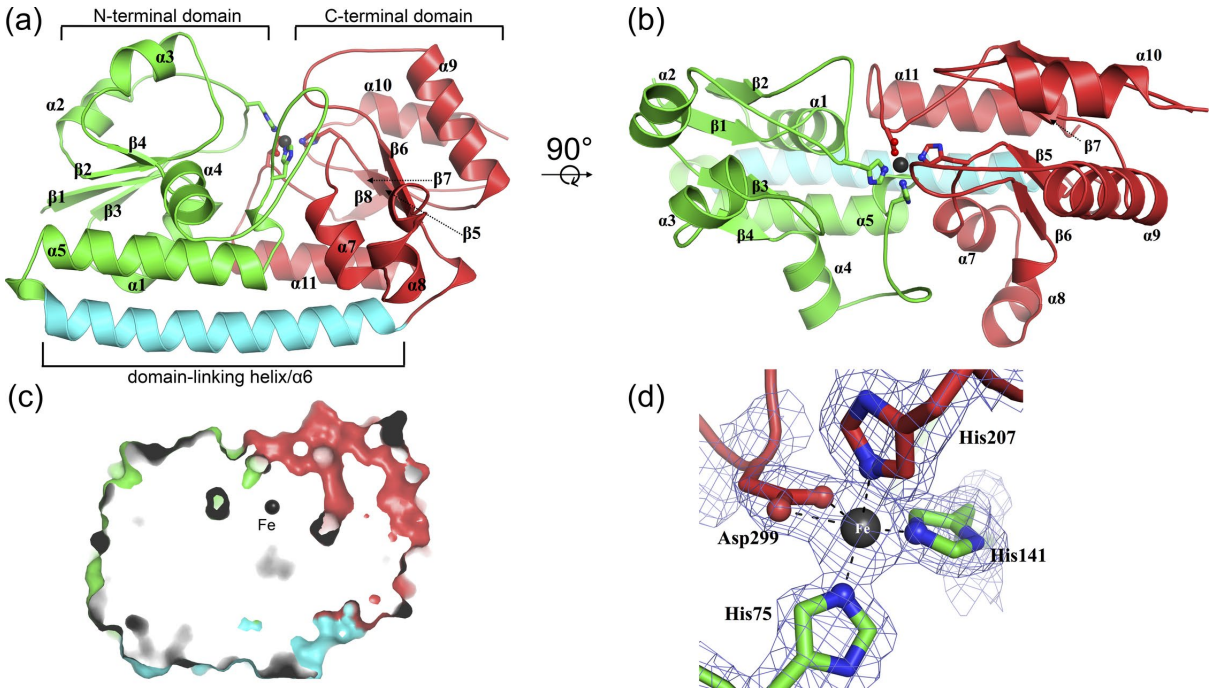


866

867

868

869 **Figure 8**

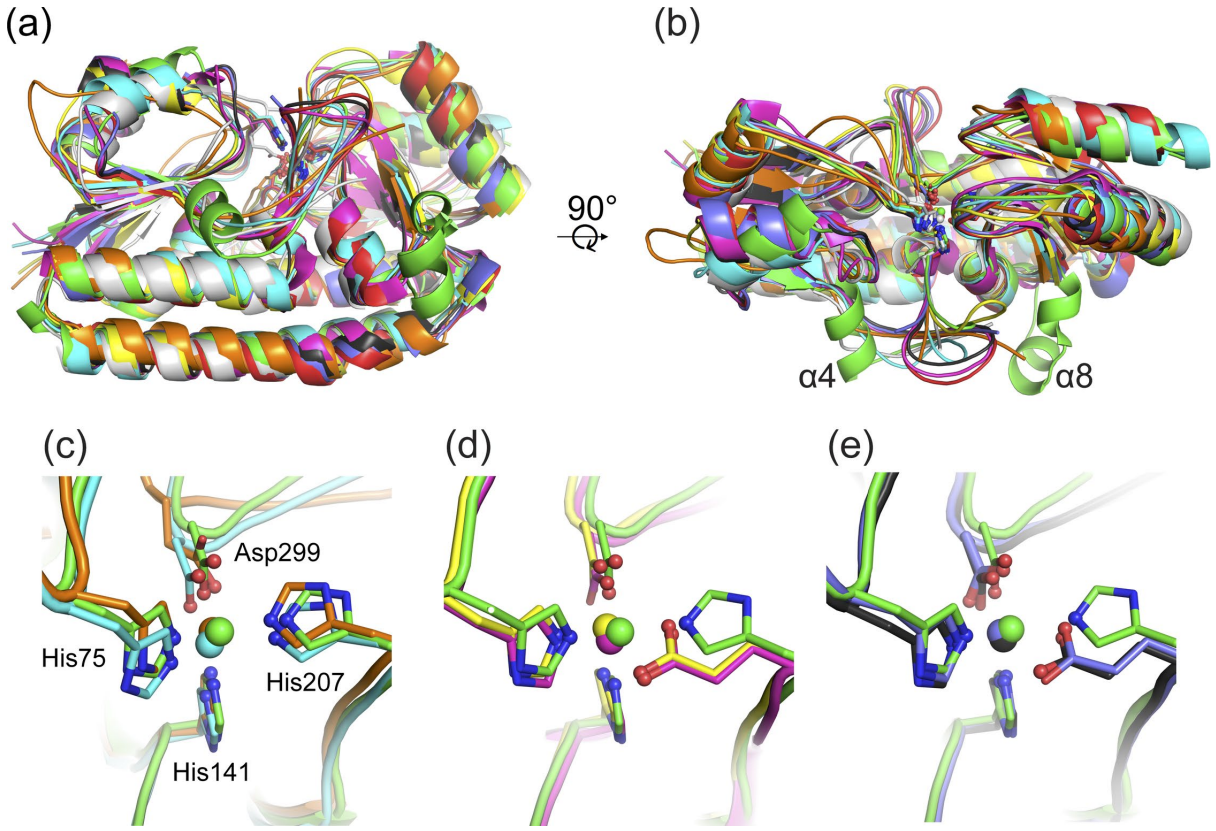


870

871